Bounding Errors Caused by Nominal GNSS Signal Deformations

Gabriel Wong, R. Eric Phelts, Todd Walter, Per Enge,
Stanford University

BIOGRAPHY

Gabriel Wong is an Electrical Engineering Ph.D. candidate at the Stanford University GNSS Research Laboratory. He has previously received an M.S.(EE) from Stanford University, and a B.S.(EECS) from UC Berkeley. His current research involves signal deformation monitoring and mitigation for GNSS signals.

R. Eric Phelts, Ph.D., is a research engineer in the Department of Aeronautics and Astronautics at Stanford University. He received his B.S. in Mechanical Engineering from Georgia Institute of Technology in 1995, and his M.S. and Ph.D. in Mechanical Engineering from Stanford University in 1997 and 2001, respectively. His research involves signal deformation monitoring techniques and analysis for SBAS, GBAS, and the GPS Evolutionary Architecture Study (GEAS).

Todd Walter, Ph.D., is a senior research engineer in the Department of Aeronautics and Astronautics at Stanford University. Dr. Walter received his Ph.D. from Stanford and is currently working on modernization of the Wide Area Augmentation System (WAAS) and defining future architectures to provide aircraft guidance. Key contributions include early prototype development proving the feasibility of WAAS, significant contribution to the WAAS MOPS, design of ionospheric algorithms for WAAS, and development of dual frequency algorithms for SBAS. He is a fellow of the Institute of Navigation and serves as its president.

Per Enge, Ph.D., is a professor of aeronautics and astronautics at Stanford University, where he is the Kleiner-Perkins Professor in the School of Engineering. He directs the GNSS Research Laboratory, which develops satellite navigation systems. He has been involved in the development of the Federal Aviation Administration's GPS Wide Area Augmentation System (WAAS) and Local Area Augmentation System (LAAS). For this work, Enge has received the Kepler, Thurlow, and Burka awards from the Institute of Navigation (ION). He received his Ph.D. from the University of Illinois. He is a member of the National Academy of Engineering and a Fellow of the IEEE and the ION.

ABSTRACT

Nominal signal deformations are present in GNSS-GPS and WAAS-GEO satellite signals. They result in pseudorange errors, which in turn cause navigation errors for GNSS users. These navigation errors depend on the user- and reference-receiver configuration parameters as well as satellite geometry and user location.

Previous papers by the authors focused on obtaining a better understanding of the pseudorange errors caused by nominal signal deformations. For this paper, we examine the user navigation error effects of nominal signal deformations from many perspectives: based on the pseudorange tracking errors from real GPS data, what would be the resultant worst case position errors? When do they become a significant integrity concern? Which user receiver configurations appear least (or most) sensitive to them? What are the effects in the dual-frequency and/ or depleted constellation configurations?

The user errors are also a function of best-case and worst-case satellite geometries at the user receiver, which are in turn dependent on user/ reference receiver locations. Nominal and degraded satellite geometries for different user locations were generated using the MATLAB Algorithm Availability Simulation Tool (MAAST) Matlab toolbox, developed at Stanford, and the best and worst case position errors were determined for these cases.

The results presented are for typical WAAS aviation users of a single-frequency, GPS-only constellation, but they can be easily extended to multiple-frequency, multi-constellation systems. These results may be especially important with the upcoming increasing availability of dual-frequency systems – the use of linear combinations of signals from the same satellite to remove ionospheric errors in turn scales the signal-deformation-induced errors.

These results indicate that for dual-frequency WAAS users, mitigation is needed to protect against navigation errors from nominal signal deformation. This paper also proposes one such practical method – augmentation of the existing Vertical Protection Level (VPL) equation with a Vertical Error Bounds for Signal Deformation (VEB$_{SD}$). This method is shown to be an effective protection mechanism.

INTRODUCTION

Signal deformations result in pseudorange errors. These errors depend on the reference and user receiver configuration parameters such as bandwidth, correlator spacing and other parameters. In turn, these errors cause position errors, whose severity depend on satellite geometry and user location.

Nominal signal deformations were previously measured and characterized for the existing constellation of GPS and WAAS-GEO satellites [4, 7]. These deformation characteristics were found to be different for each satellite signal.

The measurement and characterization process also allowed correlation peaks to be determined for each satellite. From them, pseudorange bias/ tracking error curves could be determined.

The pseudorange biases were determined using two different methods and data from two different sources: satellite-dish data processing and hardware receiver processing. Satellite-dish data processing generated pseudorange bias/ tracking error curves for all different reference receiver correlator spacings, and all user receiver correlator spacings; hardware receiver processing was only able to generate pseudorange bias/ tracking error curves for a limited number of reference- and user-receiver correlator spacings: {0.05, 0.1, 0.15, 0.2} chips. Both these methods measured pseudorange biases for all satellite signals. Results from both measurement methods showed biases which had similar ranges and trends. Other researchers have found similar results [1, 2, 3]. Additional details and further comparison were previously described [8].

In this paper, we investigated the worst case errors that resulted from these pseudorange biases; in particular, we examined the effects of the scaling caused by dual-frequency ionosphere-free combination:

$$PR_{iono-free} = \frac{f_1^2}{f_1^2 - f_5^2} PR_{L1} - \frac{f_5^2}{f_1^2 - f_5^2} PR_{L5}$$

$$\approx 2.26 \times PR_{L1} - 1.26 \times PR_{L5} \text{ --------- (1)}$$

Where

$PR_{iono-free}$: Pseudorange from dual-frequency ionosphere-free combination

f_1 : GPS L1-frequency: 1575.42 MHz

f_5 : GPS L5-frequency: 1176.45 MHz

PR_{L1} : L1-frequency Pseudorange

PR_{L5} : L5-frequency Pseudorange

The linear combination of the L1 and L5-pseudoranges has the effect of scaling random errors by a root-sum-square factor of 2.6, which we refer to, for convenience, as the dual-frequency ionosphere-free combination scaling factor. We also examined the effect of depleted constellations – up to five satellites missing from the satellite constellation. While this is exceedingly unlikely, users desiring greater immunity to errors from the ionosphere could use dual frequency L1-L5 signals and be in this situation before a full constellation of L1-L5 satellites is complete.

The process of investigation, results, observations and mitigation would be presented in subsequent sections.

DETERMINATION OF PSEUDORANGE BIASES

Pseudorange biases for the following configuration – reference-receiver correlator spacing of 0.1 chips, and for user-receiver correlator spacing of {0.05, 0.2, 0.5, 1} chips – were used for the study.

An illustration of how to obtain these desired biases is as follows: Figure **1** shows the set of pseudorange biases for the reference receiver correlator spacing of interest, processed from satellite dish data, for all satellites and all user correlator spacings from 0 to 1.2chips. The pseudorange biases at the selected user-receiver correlator spacings of {0.05, 0.2, 0.5, 1} chips are read from Figure **1** at the appropriate user-receiver correlator spacings.
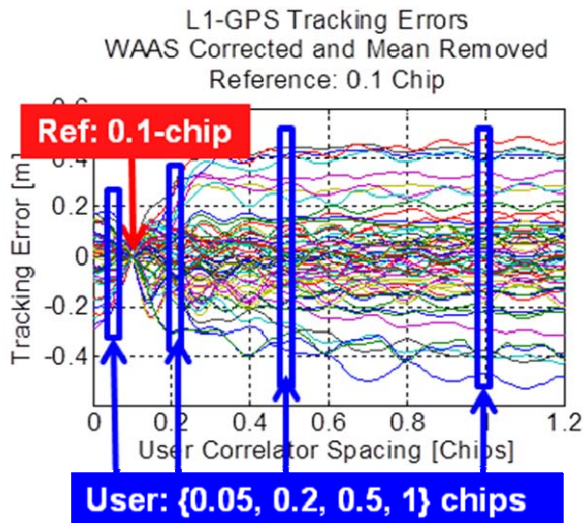
Figure **1**: Pseudorange biases corresponding to a reference-receiver correlator spacing of 0.1 chips and a user-receiver correlator spacing of 0-1.2 chips, for all GPS-GNSS satellites. These biases are obtained from processing satellite-dish data. The desired biases for the desired user-receiver correlator spacings are obtained for each satellite from this set of curves.

Biases derived from the satellite dish data tended to suffer from larger uncharacterized noise compared to the biases from hardware receiver; in contrast, biases from the hardware receiver method resulted in position errors which better matched actual user position errors. Thus these latter biases were used in the present study.

These results are summarized in the following table, for reference receiver correlator spacing of 0.1 chips, and user receiver correlator spacings of {0.05, 0.2, 0.5, 1} chips. This is the reference-receiver-user-receiver configuration we studied in greater detail.

	User Correlator Spacing [Chips]			
	0.05	0.2	0.5*	1*
Pseudo-range Biases[m]	0.1- 0.2	0.1- 0.3	0.15-0.4	0.15-0.5

Table **1**: Summary of pseudorange biases [m] for user receiver correlator spacings of {0.05, 0.2, 0.5, 1} chips. Reference receiver correlator spacing: 0.1 chips.
*Note: due to limited correlator spacings on the hardware receiver, the pseudorange biases for user correlator spacing of 0.5 and 1 chips were obtained by scaling the magnitudes of the satellite dish measurements to match the hardware receiver measurements.

POSITION ERROR COMPUTATION: SETUP

From the pseudorange errors, we could determine the worst case position errors. This is summarized in the block diagram in Figure **2**.
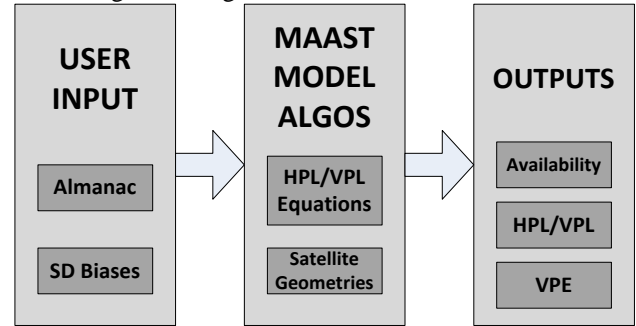

Figure **2**: Block diagram of input blocks, Matlab Algorithm Availability Simulation Tool (MAAST) process blocks and output blocks for study.

The pseudorange biases and an almanac for a particular day, Aug 03 2010, were used as input to Stanford's Matlab Algorithm Availability Simulation Tool (MAAST).

Based on the almanac, MAAST generated geometries and Vertical Protection Levels (VPL) and Horizontal Protection Levels (HPL) **[5, 6]**. MAAST also computed outputs of availability and Vertical Position Errors, together with VPLs and HPLs.

MAAST also computed other navigation errors such as clock and horizontal position errors, but in this paper we focus on the critical VPEs. These were computed by summing the products of the pseudorange bias vector elements with the vertical-position row elements of the pseudoinverse of the weighted geometry matrix:

$$VPE_{SD} = \sum_{i=1}^{N} S_{3,i} b_{SD,i} \text{ --------------------------------- (2)}$$

Where:

VPE_{SD} : Vertical Position Error for signal deformation [m]

$S_{3,i}$: vertical-position row elements of the pseudoinverse of the weighted geometry matrix.

$b_{SD,i}$: pseudorange bias vector elements [m] (obtained in the previous section) corresponding to the specific value for satellites

Figure **3** shows sample absolute VPEs computed over the course of a day for a dual-frequency configuration, for a user-receiver correlator spacing of 0.2chips.
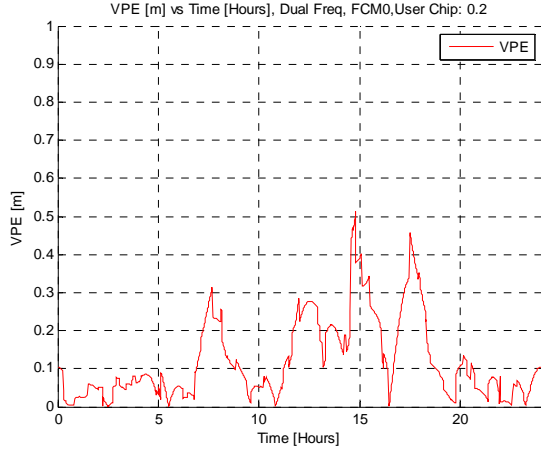
Figure 3: Time series of VPEs over the course of a day, for a dual-frequency case, full-constellation. The reference-receiver correlator spacing is 0.1 chips; the user-receiver correlator spacing is 0.2 chips.

To generate graphs of worst case errors vs percentiles – the results in the next section – these VPEs were sorted in order of magnitude, then plotted on the vertical axis vs percentiles on the horizontal axis.

To determine the effect of depleted satellite configurations, geometry matrices were first computed for all-in-view satellites subject to a mask angle of 5°. Further geometry matrices were generated for all possible combinations after satellites had been removed progressively starting one at a time and ending at five. The number of combinations for depleted constellation increases combinatorically; thus we computed the results only for a single representative location, over an entire day.

The following discusses how the VPLs and VPEs changed in the case of the dual-frequency ionosphere-free combination. These are the single- and dual-frequency VPL equations:

$$VPL_{\sin gle\_freq} = K_{v,PA}\sqrt{\sum_{i=1}^{N} S_{3,i}^2 \sigma_{\sin gle\_freq,i}^2} \text{ ------ (3)}$$

$$VPL_{dual\_freq} = K_{v,PA}\sqrt{\sum_{i=1}^{N} S_{3,i}^2 \sigma_{dual\_freq,i}^2} \text{ --------- (4)}$$

σ_{air}^2 and σ_{UIVE}^2, are two of the constituent terms of $\sigma_{\sin gle\_freq,i}^2$. In the dual-frequency, ionosphere-free configuration, σ_{air}^2 is scaled by the dual-frequency ionosphere-free combination scale factor of 2.6, and σ_{UIVE}^2 is not present due to the removal of ionospheric threat. The net effect of these two changes was to reduce the overall VPL in the dual-frequency case. This in turn

allowed more poor geometries into the dual-frequency ionosphere-free position solution; the consequences on the VPEs will be discussed further in the next section.

The dual-frequency ionosphere-free combination also caused the VPEs to be scaled by 2.6. b_{SD}, the pseudorange bias vector, was first scaled by the dual-frequency ionosphere-free combination scale factor of 2.6; this in turn scaled the VPEs by the same factor. However, as presented in the next section, in the case of dual-frequency depleted-geometry configurations, the worst-case VPEs were inflated by more than this scale factor.

POSITION ERRORS RESULTS – INTEGRITY

All results in this section are for a single location and over an entire day, for a reference receiver of 0.1chip correlator spacing.

Figure 4 shows the worst case errors for a **single frequency** full constellation configuration. The availability was 100.0% and the worst case errors were approximately 0.3m.
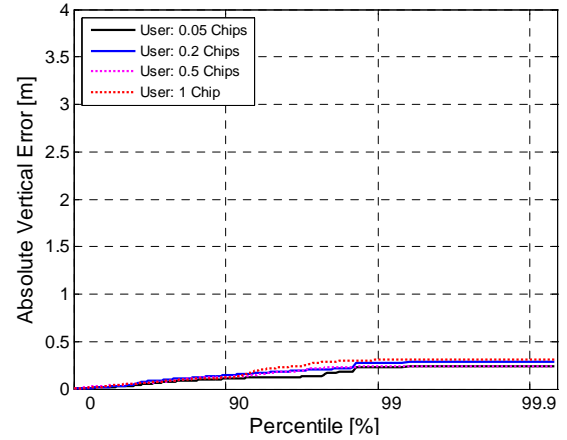

Figure 4: Single frequency, full constellation. Availability: 100.0%. Worst-case vertical error: ~0.29m [0.2chips], ~0.31m [1 chip]

Figure 5 shows the worst case errors for a **dual frequency** full constellation case. The availability was 100.0% – not lower than the single frequency case – and the worst case errors were approximately 0.5m. These errors were larger and largely caused by the dual-frequency ionosphere-free combination scaling.
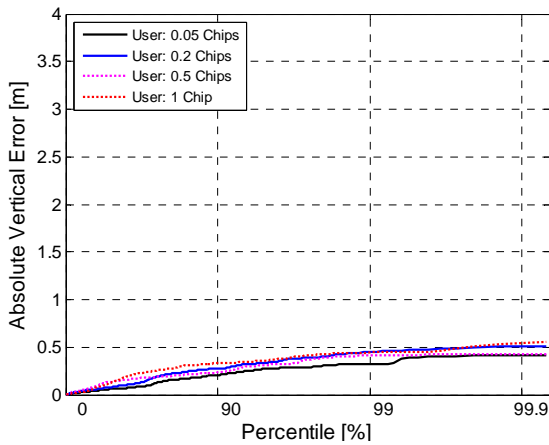
Figure 5: Dual frequency, full constellation. Availability: 100.0%. Worst-case vertical error: ~0.51m [0.2chips], ~0.56m [1 chip]

Figure 6 shows the worst case errors for a **single frequency** constellation-minus-1 configuration (all possible combinations of 1 missing satellite from the constellation). Compared to the full constellation case, the availability decreased to 95.0%, and the worst case errors slightly increased. This was due to the occurrence of poorer geometries – leading to exclusion of some geometries under LPV200 and poorer availability. The poorer geometries also caused an increase in DOP and worse user-position errors.
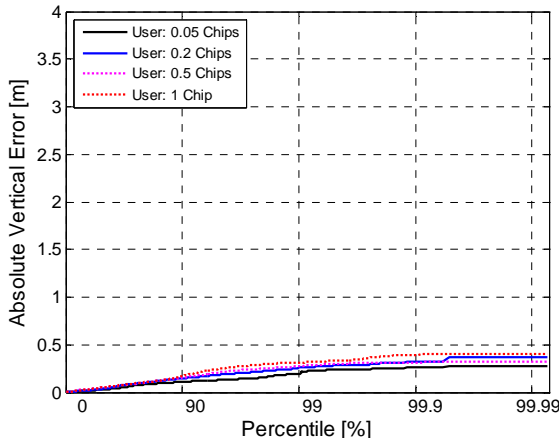

Figure 6: Single frequency, constellation: 1-missing. Availability: 95.0%, Max error: ~0.37m [0.2chips], ~0.4m [1 chip]

Figure 7 shows the worst case errors for a **dual frequency** constellation-minus-1 case. The availability was 100.0% and the worst case errors were between 1.27m and 2.7m. In this case, the worst case errors increased by a scale factor range of 4 to 6, more than would be expected due to the dual-frequency ionosphere-free combination scaling of 2.6. This was caused by the increased availability – due to lower fault-free VPLs for dual-frequency, degraded geometries which would have been

excluded in the single frequency case were now admitted. This resulted in additional degradation in worst case errors.
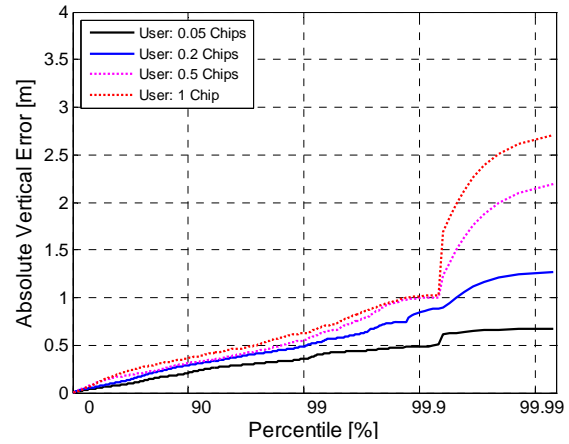

Figure 7: Dual frequency, constellation: 1-missing. Availability: 100.0%, Worst-case vertical error: ~1.27m [0.2chips], ~2.7m [1 chip]

Figure 8 shows the worst case errors for a **single frequency** constellation-minus-5 case (all possible combinations of 5 missing satellite from the constellation). Compared to the single frequency full constellation and constellation-minus-one cases, the availability and worst case errors followed similar trends – degradation in availability and worst case vertical errors – as more satellites were removed. The availability was now 38.2% and the worst case errors were now between 0.35m and 0.7m.
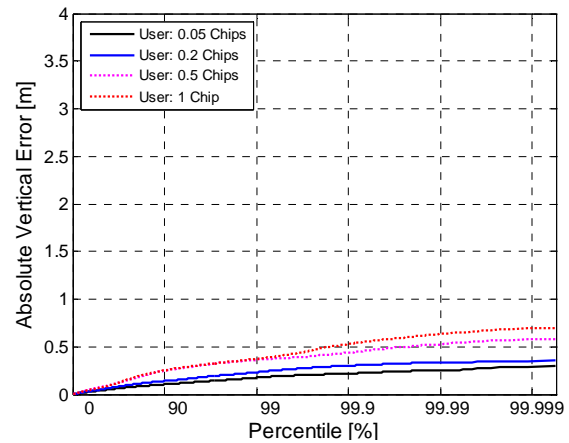

Figure 8: Single frequency, constellation: 5-missing. Availability: 38.2%, Worst-case vertical error: ~0.35m [0.2chips], ~0.7m [1 chip]

Figure 9 shows the worst case errors for a **dual frequency** constellation-minus-5 configuration (all possible combinations of 5 missing satellite from the constellation). Compared to the single frequency case, as in previous cases, the availability was now much higher – 92.2% vs 38.2%, but the worst case errors were now

much worse – between 1.89m and 3.86m. The same explanation as in the previous configuration of constellation-minus-1 held true: lower fault-free VPLs in the dual-frequency case admitted more degraded geometries, resulting in higher availability at a cost of degraded worst-case position errors.
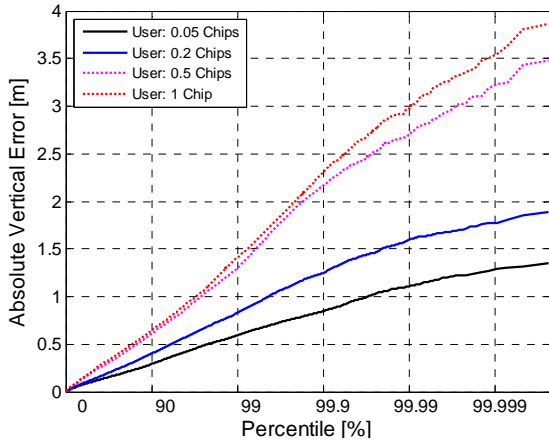

Figure **9**: Dual frequency, constellation: 5-missing. Availability: 92.2%, Worst-case vertical error: ~1.89m [0.2chips], 3.86m [1 chip]

Table **2** summarizes the effect of depleted geometry and dual-frequency ionosphere-free combination on worst case errors and availability, for correlator spacings of 0.1 chip for reference receiver and 0.2 chips for user receiver.

#Missing Satellites	SINGLE FREQUENCY			DUAL FREQUENCY		
	Avail	Position Errors [m]		Avail	Position Errors [m]	
		99%	Max		99%	Max
0	100.0%	0.28	0.29	100.0%	0.45	0.51
1	95.0%	0.26	0.37	100.0%	0.49	1.27
2	85.5%	0.26	0.38	99.9%	0.57	1.50
3	71.6%	0.26	0.35	99.3%	0.66	1.56
4	54.5%	0.25	0.37	97.4%	0.73	1.68
5	38.2%	0.23	0.35	92.2%	0.83	1.89

TABLE **2**: Effect of depleted satellite geometry on availability and worst case vertical errors, for both single and dual frequency. Correlator spacing: 0.1 chip for reference receiver, 0.2 chips for user receiver.

As the number of available satellites decreased, in the single-frequency case the worst case errors remained the same, but the availability dropped significantly. In the dual frequency case, the availability degraded slightly, at the cost of worst-case errors that at least quadrupled.

Table **3** is similar to the Table 2; the only difference is that the results are for user receiver correlator spacing of **1 chip.**

#Missing Satellites	SINGLE FREQUENCY			DUAL FREQUENCY		
	Avail	Position Errors [m]		Avail	Position Errors [m]	
		99%	Max		99%	Max
0	100.0%	0.30	0.31	100.0%	0.44	0.56
1	95.0%	0.31	0.40	100.0%	0.63	2.70
2	85.5%	0.34	0.49	99.9%	0.80	3.09
3	71.6%	0.36	0.63	99.3%	0.97	3.40
4	54.5%	0.37	0.69	97.4%	1.18	3.81
5	38.2%	0.37	0.70	92.2%	1.40	3.86

TABLE **3**: Effect of depleted satellite geometry on availability and worst case vertical errors, for both single and dual frequency. Correlator spacing: 0.1 chip for reference receiver, 1 chip for user receiver.

In this case, the availability and worst-case error trends were identical to that shown in the previous table – constant worst-case errors and poor availability in the single-frequency case, and much better availability, but much degraded worst-case errors in the dual-frequency case. In addition, using a wider correlator spacing of 1 chip in the user receiver resulted in a further increase (doubling) of the error.

This section has shown that dual frequency SBAS users could experience worst case errors that more than quadruple. This is due to two cumulative effects: the scaling due to dual-frequency ionosphere-free combination; and more poor geometries entering into the position solutions due to lower VPLs in the dual frequency case. In addition, using a user-receiver correlator spacing of 1-chip resulted in an error that approximately doubles compared to the 0.2-chip user receiver correlator spacing.

This highlights the necessity of protecting SBAS users, especially in dual-frequency configurations, from the adverse effects of worst case errors caused by nominal signal deformation. Simply lowering the Vertical Alarm Limit (VAL) could protect against these errors, but would lead to loss of availability. A more effective way to protect against these worst-case errors specific to signal deformation, while minimizing loss of availability, is presented in the next section.

PROTECTION MECHANISM

The previous section highlighted the need to protect against signal-deformation-induced worst-case position errors to maintain integrity without losing availability.

Two different Vertical Error Bounds for Signal Deformation (*VEB*$_{SD}$) were examined in detail; the results are presented in this section.

The first error bound $VEB_{SD,1}$ was obtained by summing the absolutes of the products of the pseudorange bias vector elements with the vertical-position row elements of the pseudoinverse of the weighted geometry matrix.
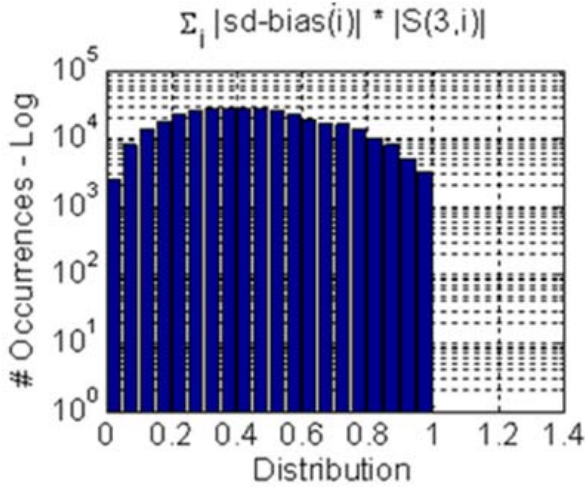
$$VEB_{SD,1} = \sum_{i=1}^{N} | S_{3,i} b_{SD,i} | \text{ ----------------------------- } (5)$$

Where:

$VEB_{SD,1}$	:	Vertical Error Bound for signal deformation [m]
$S_{3,i}$	:	vertical-position row elements of the pseudoinverse of the weighted geometry matrix.
$b_{SD,i}$	:	pseudorange bias vector elements [m]

Figure 10: Histogram of the ratio of VPEs to $VEB_{SD,1}$. Note that the ratios were less than or equal to 1.

The histogram in **Figure 10** shows the performance of $VEB_{SD,1}$. This would have been an almost ideal error bound for integrity – the ratio of vertical errors to $VEB_{SD,1}$ approached but never exceeded unity. However, computing this bound requires knowledge of each bias magnitude, which would be impractical in actual implementation.

The next error bound $VEB_{SD,2}$ was obtained by multiplying the maximum of the absolute values of the pseudorange bias vector elements with the sum of the absolutes of the vertical-position row elements of the pseudoinverse of the weighted geometry matrix.
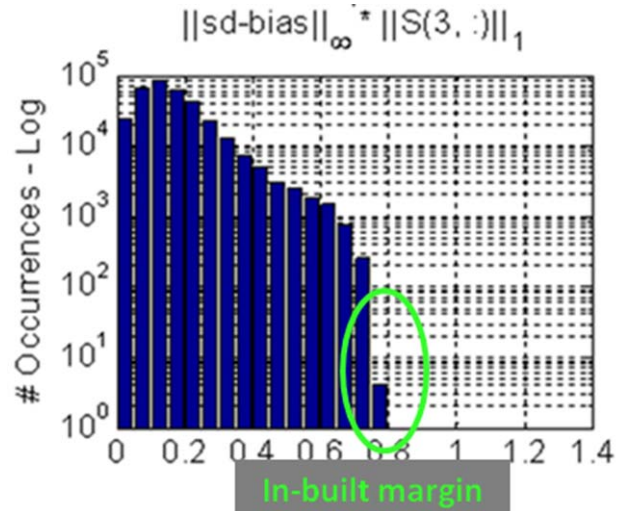
$$VEB_{SD,2} = \| b_{SD} \|_{\infty} \times \sum_{i=1}^{N} | S_{3,i} | \text{ ------------------ } (6)$$

Where:

$VEB_{SD,2}$	:	Vertical Error Bound for signal deformation [m]
$S_{3,i}$	:	vertical-position row elements of the pseudoinverse of the weighted geometry matrix.
$\|b_{SD,i}\|_{\infty}$	:	maximum of absolute pseudorange bias vector elements [m]

Figure 11: Histogram of the ratio of VPEs to $VEB_{SD,2}$. Note that the ratios never exceeded 0.8.

The histogram in **Figure 11** shows the performance of $VEB_{SD,2}$. The ratio of vertical errors to $VEB_{SD,2}$ did not exceed 0.8; thus $VEB_{SD,2}$ protected adequately against worst-case pseudorange errors from signal deformation. $VEB_{SD,2}$ was conservative – it provided a built-in safety margin, at the expense of some loss of availability compared to $VEB_{SD,1}$. It was also practical to implement – simply requiring an estimate or specification of the largest of the signal deformation biases amongst all satellites for a particular reference-receiver-user-receiver configuration.

The proposed protection mechanism would be to augment the existing VPL equation with the new error bound:

The original fault-free dual-frequency VPL, as before:

$$VPL_{dual\_freq} = K_{v,PA} \sqrt{\sum_{i=1}^{N} S_{3,i}^2 \sigma_{dual\_freq,i}^2} \text{ -------- } (4)$$

New proposed dual-frequency VPL:

$$VPL_{dual\_freq} = K_{v,PA} \sqrt{\sum_{i=1}^{N} S_{3,i}^2 \sigma_{dual\_freq,i}^2} + \| b_{SD} \|_{\infty} \times \sum_{i=1}^{N} | S_{3,i} | \quad (7)$$

where the additional term is $VEB_{SD,2}$

Some ad-hoc bounds have also been suggested as approximate bounds for the VPEs that could be lower than $VEB_{SD,1}$ and $VEB_{SD,2}$; two such bounds were examined and described here. It was found that both bounds did not bound the VPEs all of the time.

The bounds that were examined include: product of absolutes of maximum of bias vector and maximum of vertical-position row elements of the weighted geometry matrix (equation **8**); product of maximum of bias vector

and sum of 4 largest absolute vertical-position row elements of the weighted geometry matrix (equation **9**).

$$VEB_{SD,3} = \| b_{SD} \|_\infty \times \| S_3 \|_\infty \text{---------------------} \quad (8)$$

$$VEB_{SD,4} = \| b_{SD} \|_\infty \times \sum_{i=1}^{4} | S_{3,sort,i} | \text{------------} \quad (9)$$

Where:

$VEB_{SD,3}$: Unsuitable Vertical Error Bound for signal deformation [m]

$VEB_{SD,4}$: Unsuitable Vertical Error Bound for signal deformation [m]

$\| b_{SD,i} \|_\infty$: maximum of absolute pseudorange bias vector elements [m]

$S_{3,i}$: vertical-position row elements of the pseudoinverse of the weighted geometry matrix.

$S_{3,sort,i}$: vertical-position row elements of the pseudoinverse of the weighted geometry matrix, sorted by absolute value, in decreasing order.

In the first case, as was expected, the VPEs often exceeded $VEB_{SD,3}$. In the second case, the VPEs exceeded the $VEB_{SD,4}$ in some cases. Thus both these bounds were found to be unsuitable.

CONCLUSION

Nominal signal deformations cause pseudorange biases which in turn lead to position errors. The effect on worst-case position errors for dual-frequency, ionosphere-free combination users compared to single-frequency users was studied and the results presented in this paper. This study was done for a wideband reference receiver with a correlator spacing of 0.1 chips and user receiver of the same bandwidth and a correlator spacing of {0.05, 0.2, 0.5, 1} chips, as well as for increasingly-degraded satellite geometries – from a full constellation to a constellation with 5 missing satellites.

The results show that, with as few as 1 missing satellite, dual-frequency users could experience a worst-case vertical position error that was 4-6x that of the single-frequency user. This was both caused by the scaling from dual-frequency ionosphere-free scaling, as well as the admission of degraded geometries due to the lowering of fault-free VPLs for the dual-frequency case. Use of wide correlator spacing in the user receiver caused a further doubling of the error compared to narrow correlator spacing. With the cumulative effects of the scaling, errors which were previously insignificant now became significant in the dual-frequency case. This highlighted the need for a protection mechanism to mitigate against such errors.

Two vertical error bounds for signal deformation, $VEB_{SD,1}$ and $VEB_{SD,2}$, were proposed as augmentations to the existing fault-free VPL equation. The first worked well but was impractical to implement. The second was practical but conservative – incorporating a built-in margin at the cost of some availability. Both these vertical error bounds provided safe protection against the signal deformation vertical position errors.

REFERENCES

[1] Brenner, M., Kline, P., Reuter, R., "Performance of a Prototype Local Area Augmentation System (LAAS) Ground Installation", Proceedings of ION GPS 2002, Portland, OR, Sep 2002

[2] Hegarty, Christopher J., Van Dierendonck, A.J., "Recommendations on Digital Distortion Requirements for the Civil GPS Signals," Proceedings of IEEE/ION PLANS 2008, Monterey, CA, May 2008

[3] Phelts, R.E., "Nominal Signal Deformations: Limits on GPS Range Accuracy", The 2004 International Symposium on GPS/GNSS, Sydney, Australia, December 2004

[4] Phelts, R. E., Walter, T., Enge, P., "Characterizing Nominal Analog Signal Deformations on GNSS Signals", Proceedings of the 22nd International Technical Meeting of The Satellite Division of the Institute of Navigation (ION GNSS 2009), Savannah, GA, September 2009

[5] Walter, Todd, Enge, Per, Hansen, Andrew, "A Proposed Integrity Equation for WAAS MOPS", Proceedings of the 10th International Technical Meeting of the Satellite Division of The Institute of Navigation (ION GPS 1997), Kansas City, MO, September 1997, pp. 475-484.

[6] Walter, T., Blanch, J., Enge, P., "Vertical Protection Level Equations for Dual Frequency SBAS", Proceedings of the 23rd International Technical Meeting of The Satellite Division of the Institute of Navigation (ION GNSS 2010), Portland, OR, September 2010, pp. 2031-2041.

[7] Wong, G., Phelts, R.E., Walter, T., Enge, P., "Characterization of Signal Deformations for GPS and WAAS Satellites", Proceedings of the 23rd International Technical Meeting of The Satellite Division of the Institute of Navigation (ION GNSS 2010), Portland, September 2010

[8] Wong, G., Phelts, R.E., Walter, T., Enge, P., "Alternative Characterization of Analog Signal Deformation for GNSS-GPS Satellites", Proceedings of